Reactive precipitation of vaterite calcium carbonate microspheres in supercritical carbon dioxide-water dispersion by microfluidics

Pierre Legout, Guillaume Lefebvre, Marie Bonnin, Jean Christophe Gimel, L. Benyahia, Alain Gibaud, Samuel Marre, Carl Simonsson, Sébastien Wang, Olivier Colombani, et al.

Reactive precipitation of vaterite calcium carbonate microspheres in supercritical carbon dioxide-water dispersion by microfluidics

Pierre Legout[1, 2], Guillaume Lefebvre[1], Marie Bonnin[1], Jean-Christophe Gimel[1], Lazhar Benyahia[2], Alain Gibaud[2], Samuel Marre[3], Carl Simonsson[1], Sébastien Wang[1], Olivier Colombani[2] and Brice Calvignac[1*]*

[1]Univ Angers, Inserm, CNRS, MINT, SFR ICAT, F-49000 Angers, France

[2]Institut des Molécules et Matériaux du Mans (IMMM), UMR 6283 CNRS, Le Mans Université, Avenue Olivier Messiaen, 72085 Le Mans Cedex 9, France.

[3]CNRS, Univ. Bordeaux, Bordeaux INP, ICMCB, UMR5026, 33600 Pessac

ABSTRACT

Vaterite, a polymorphic form of precipitated calcium carbonate, is an interesting material for various applications such as formulation of drug delivery systems due to its nanoporous structure. One of the carbonation processes to obtain nanostructured microspheres of vaterite consists in mixing an aqueous calcium phase with a supercritical CO_2 phase, resulting in a heterogeneous dispersion. In this study, a continuous microfluidic method has been evaluated to produce monodisperse porous vaterite microparticles. A high-pressure microfluidic set-up has been developed, revealing that the dimensions and the dispersity of the $CaCO_3$ particles are not affected by pressure but can be decreased by increasing the flow rate of the $scCO_2$ and aqueous phases or addition of polymers in the aqueous phase. These observations were shown not to be related to the degree of dispersion of each phase within the microfluidic channel but to the interaction of the polymer with the $CaCO_3$ particles and to the depressurization step at the end of the channel.

KEYWORDS. calcium carbonate, supercritical carbon dioxide, microfluidics, polymer, polydimethyl siloxane, vaterite

PUBLISHED IN The Journal of Supercritical Fluids 188 (2022) 105678

https://doi.org/10.1016/j.supflu.2022.105678

Introduction

Calcium carbonate ($CaCO_3$) is an abundant granular material used as additive in food ingredients, cosmetics, agricultural and pharmaceutical products, but also as filler and pigment for coatings, paper, plastics, rubber, adhesives, textiles, building materials, glass and ceramics.[1] The global $CaCO_3$ market is split between Ground Calcium Carbonate (GCC) and Precipitated Calcium Carbonate (PCC). At the industrial scale, GCC is obtained by mining limestone deposits, and PCC is produced by the chemical reaction of $Ca(OH)_2$ with CO_2. GCC is more widely used – 60 million tons per year against 14 million tons for PCC – because it is cheaper to produce and naturally abundant. However, limestone deposits consist of the most thermodynamically stable crystalline form of $CaCO_3$, namely calcite, thus only yields this allotropic state.

On the contrary, PCC can be manufactured under specific and controlled operating conditions, allowing the tuning of its characteristics in terms of polymorphism (calcite, aragonite, vaterite – from the most stable to the least stable form), morphology, structure, porosity and granulometry.[1] Vaterite is thermodynamically unstable, but unlike calcite and aragonite, it spontaneously exhibits a hollow core and nanoporous structure,[2] a high surface area and a tunable morphology and size. It is therefore a highly relevant carrier for drug delivery applications, as this kind of nanostructure allows high encapsulation efficiency and is well adapted for controlled drug release.[2,3,4] According to the Ostwald-Lussac law, the metastable vaterite is obtained before the most thermodynamically stable form (calcite) and tends to evolve towards it. To prepare vaterite, the challenge is thus to achieve its formation through an appropriate PCC process while preventing its transformation into calcite to take advantage of its porosity for drug delivery. To this end, additives such as polysaccharides, block copolymers, proteins, amino acids, peptides, alcohols, phospholipids or surfactants are added to the carbonation reaction mixture to preferentially orientate the vaterite precipitation.[5] Our previous works showed that glycine is particularly efficient to produce vaterite particles that are stable for many months once freeze-dried.[6] It should be noticed that vaterite can also be obtained without any additives using highly supersaturated and perfectly controlled hydrodynamic conditions.[7]

Regardless of the desired polymorphic PCC form, calcium carbonate is generally obtained chemically by simply mixing calcium and carbonate salts in an aqueous medium. In the literature, different reactive precipitation strategies have been proposed to control the polymorphism and granulometry of PCC during the carbonation process: the CO_2 bubbling method and the supercritical CO_2 ($scCO_2$) route,[8] the emulsion (double emulsions[9,10] or microemulsions[11,12,13,14,15,16,17]) mixing processes, the solvothermal synthesis[17] and the biomineralization method with bacteria.[18] Among the different reactive precipitation processes, the $scCO_2$ route is of particular interest. In this process, the $scCO_2$ is acting as a dispersive phase as well as the carbonate source. It consists in pressurizing a stirred Ca^{2+} aqueous phase with $scCO_2$ during a specific time at a pressure where CO_2 is supercritical and dissolves sufficiently in the aqueous phase to decrease its pH and prevent $CaCO_3$ precipitation. Then, depressurization without stirring induces a pH increase. This triggers the formation of CO_3^{2-} ions, coming from CO_2, which interact with Ca^{2+} and form the $CaCO_3$ particles. The use of $scCO_2$ enables a high supersaturation of the CO_2, and thus of the carbonate ions, in a reactive aqueous phase, making it more favorable for vaterite obtention.[19,20] The $scCO_2$ is also a variable geometry green solvent allowing to tune the carbonation conditions by changing P or T. Finally, the $scCO_2$ route is a low energy-consuming and a volatile organic compound-free process leading to good carbonation yields.[20,21,22] However, the current $scCO_2$ batch process patented by our team[23] has several drawbacks. Mechanical stirring is used to saturate the calcium solution with CO_2, and it is stopped before depressurization of the autoclave for $CaCO_3$ precipitation. Such a process in a high-pressure batch reactor is therefore time-consuming and does not allow a precise control of the size and dispersity of the formulated particles due to possible batch-to-batch variations. Finally, the scale-up of such batch processes remains a challenge.

Continuous microreactors present high reproducibility, low batch-to-batch variations, narrower and better control of the particle size distribution, and an easier scale-up.[24] Thus, to overcome the batch process drawbacks without giving

up the advantages of $scCO_2$, the original combination of an $scCO_2$-water emulsification route and a continuous microfluidic process seems to be a time saving and more scalable alternative. In the present work, we investigated for the first time the precipitation of $CaCO_3$ in the vaterite form by an original low energy continuous microfluidic process using a water-$scCO_2$ (W-C) dispersion. We note that for the vaterite precipitation, batch processes under ambient pressure and temperatures between 25 and 50°C[25] were mainly investigated. Very few works have been carried out on carbonation under high pressure as in $scCO_2$ media[19,6,26] or with continuous processes such as microfluidics.[27,28,29,30] Consequently, works about continuous/microfluidic supercritical route for formulation of emulsions,[31] particle design and synthesis applications[32,33,34,35] are scarce. These processes use organic solvents and/or anti-solvent effect processes, which may raise toxicity issues and imply difficult cleaning steps for a pharmaceutical use.

The original continuous supercritical carbonation route studied here consists first in introducing separately in a specific high-pressure setup a Ca^{2+} aqueous phase and a pure $scCO_2$ phase into a micromixer. The $CaCO_3$ microparticles are formed at the end of the microfluidics channel upon depressurization using an automated pressure regulator. Since the $scCO_2$ and aqueous phase are heterogeneously dispersed in these conditions, we wondered whether the dispersion state, among other parameters, would impact the characteristics of the $CaCO_3$ particles. It was indeed suggested for microemulsion processes, which also occur in heterogeneous conditions, that the dispersion state impacts the characteristics of the $CaCO_3$ particles. Microemulsion processes usually imply mixing two microemulsions consisting of reverse micelles containing respectively aqueous calcium and carbonate salt phases. Upon mixing the microemulsion containing carbonate ions with the one containing calcium ions, the aqueous domains merge together leading to final aqueous droplets exhibiting sizes in the same range as the obtained $CaCO_3$ microparticles.[11,12,16,17,36] The initial reverse micelles (in the nanometer range) are therefore much smaller than the final $CaCO_3$ particles (from hundreds of nanometers to few micrometers).[11,13,16,36] Moreover, the number of merged droplets does not vary in a consistent way as a function of the formulation conditions, so that it does not seem possible to predict the dimensions of the $CaCO_3$ particles as a function of the initial dimensions of the microemulsions. Still, Kang et al.[36] and Kandori et al.[16] observed that decreasing the initial size of the domains forming the microemulsions (by addition of surfactant) qualitatively led to smaller diameters of the final $CaCO_3$ microparticles, allowing some control, although not predictable, over the dimensions of the $CaCO_3$ particles. In summary, results reported with microemulsion processes suggest that the dispersion state of the microemulsion impacts the dimensions of the $CaCO_3$ particles although the correlation between both aspects is currently not understood. These results led us to investigate whether the dispersion state could impact the dimensions of $CaCO_3$ particles in a $scCO_2$-water dispersion microfluidic process. Besides, we studied the influence of the pressure, flow rates of both phases, type of micromixer (coflow[37,38,39] or static) and presence of polymers to impact the dispersion state of both phases and understand whether this plays a role on the dimensions of the $CaCO_3$ particles, the carbonation yield and the polymorphism of the particles.

Materials and methods

Materials

Anhydrous calcium hydroxide $CaCl_2$ (Prolabo), CO_2 (Linde), dextrans (M_w = 40,000 and 500,000 g/mol, Sigma-Aldrich), Fluorescein isothiocyanate labeled dextran (FITC-dextran, M_w = 40,000 g/mol, Sigma-Aldrich), MilliQ water (resistivity = 18 MΩ.cm, Millipore), Glycine (Sigma-Aldrich), HCl (2 mol/L, Acros Organics), NaOH (2 mol/L, Fine Chemicals), Pluronic® PE6400 (poly(ethylene oxide)$_{13}$-*block*-poly(propylene oxide)$_{30}$-*block*-poly(ethylene oxide)$_{13}$ = PEO_{13}-PPO_{30}-PEO_{13} where the subscripts denote the number average degrees of polymerization of each block, BASF) were used as received. Poly(dimethyl siloxane)$_{13}$-*block*-poly(oligoethyleneglycol methacrylate 300)$_x$, $PDMS_{13}$-*b*-$POEGMA_x$, where the subscripts denote the number average degrees of polymerization of each block with x = 16, 31 or 46 and 300 g/mol corresponds to the number average molar mass of the OEGMA monomer, were synthesized by Radical Addition Fragmentation Transfer polymerization (RAFT) as previously reported.[40] A $POEGMA_{46}$ homopolymer was also prepared with the same method. PEO_{13}-PPO_{30}-PEO_{13}, $PDMS_{13}$-*b*-$POEGMA_x$ and $POEGMA_{46}$ are monodisperse (Đ ~ 1.1), whereas the dextrans are polydisperse polymers.

Preparation of the aqueous solution

An aqueous solution containing the Ca^{2+} ions is used both for the continuous microfluidic process and the batch process. This aqueous solution contains 1 mol/L of glycine and calcium chloride $CaCl_2$ (1.6 wt%, 0.145 mol/L Ca^{2+}). Its pH is adjusted to 10 with a 1 mol/L

NaOH solution. When a polymer is used, it is directly dissolved in the $CaCl_2$ solution at a concentration of 1 wt%.

Precipitation of calcium carbonate particles by microfluidics

In a typical microfluidic process, the previously prepared aqueous solution containing Ca^{2+} ions and $scCO_2$ are injected at fixed flow rates and pressure within a microfluidic micromixer (Fig. 1). Glycine, which is solubilized in the aqueous phase, orients the crystallization towards the vaterite polymorph.[6, 22,41,42,] The aqueous solution of $CaCl_2$ is injected by an HPLC pump (Model PU-2080, JASCO, Japan). $ScCO_2$ is injected with a syringe pump (Model 100DX, ISCO, USA) equipped with a double jacket maintained at 4°C by a thermostatic bath (Isotemp 4100R20, France). The pumps are connected to the micromixer by PEEK (poly-ether-ether-ketone) tubing and high-pressure fittings (VICI Valco Instruments, USA). Two micromixers were studied. The coaxial micromixer is a system containing a stainless-steel tube ($Ø_{int}$ = 100 µm and $Ø_{ext}$ = 500 µm) in a sapphire capillary ($Ø_{int}$ = 750 µm and $Ø_{ext}$ = 1,570 µm) that was previously described in the literature.[38] The T-shaped static micromixer (45° angle, $Ø_{int}$ = 500 µm) is made of PEEK and consists of a 10 µm frit at the outlet (IDEX U-466-02, Lake Forest, Illinois, USA). In order to control the temperature of the system, the microfluidic capillaries are thermalized by a "heating cartridge" system (manufactured by 3D printing) integrating a counter-current water circulation through a bath thermostatically controlled at 40°C (see Appendices, section 1). In addition, all the connections are also thermalized at 40°C with a counter-current tubular heat exchanger system with water circulation provided by this same thermostatic bath. The pressure is controlled using an automated pressure regulator (Model BP-2080, JASCO, Japan), needle valve type, downstream of the microfluidic system. The needle frequency was fixed on the "high level" (value not provided by the supplier) of the device for all the experiments. The valve body is heated to 80°C to prevent the formation of ice due to the cooling of the mixture by adiabatic expansion (Joule-Thomson effect) which would cause the obstruction of the nozzle of the pressure regulator. In these conditions, no plugging problems were observed. Flow rates which have been studied both for the aqueous phase and for the $scCO_2$ phase range from 1 to 8 mL/min. The videos of the flow of the two phases were taken using a high-speed Phantom Miro 110 camera (Vision Research Inc., New Jersey, USA) at a rate of 3,000 frames per second and a resolution of 1,280x440 pixels by illuminating the sapphire tube with LED lamps. Note that videos were taken at a fixed position for all experiments because of the absence of significant flow modification and dispersion state along the sapphire capillary. A volume of around 20 mL of aqueous suspension containing the calcium carbonate particles is recovered at the end of the microfluidic channel and then centrifuged at 4,000 rpm for 10 min. The supernatant is removed, and the particles are washed with 50 mL of MilliQ water, then centrifuged again at 4,000 rpm for 10 min. The centrifugation pellet of about 100 mg of particles is collected in 1 mL of MilliQ water and lyophilized.

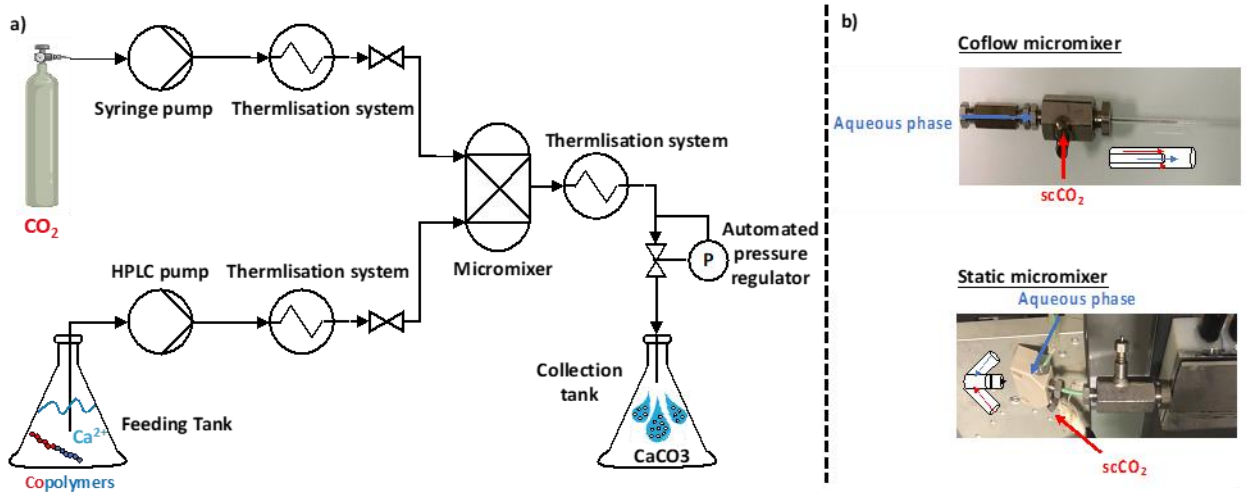

Fig. 1. a) Microfluidic pilot setup equipped with a micromixer for the continuous formulation of $CaCO_3$ microparticles in $scCO_2$-water dispersion with b) a coflow or a static micromixer.

Precipitation of calcium carbonate particles by batch

The batch process used to synthetize $CaCO_3$ particles has been studied and patented by Tewes et al. (2009)[6] and published by Beuvier et al. (2011).[22] The precipitation is conducted in a 500 mL autoclave (Separex, France) heated to 40°C, pressurized with CO_2 at 200 bar and mechanically stirred with an anchor. The initially liquid CO_2 is injected by a high-pressure diaphragm pump (Milton Roy Europe, France). As soon as thermodynamic equilibrium in pressure and temperature is reached in the autoclave, 25 mL of the aqueous Ca^{2+} solution previously prepared as described above are injected by an HPLC pump or by an ISCO 100 DX pump. The injection rate is set at 10 mL/min. Once the addition has been made, the pressure is 240 bar and the stirring is maintained at 1,200 rpm for 5 min. After stopping the agitation, the autoclave is manually depressurized for 5 min using a valve. Thereafter, the suspension of $CaCO_3$ microparticles is collected and centrifuged at 2,400g for 10 min. Lastly, microparticles are washed with 50 mL of ultrapure water (Millipore, Molsheim, France), and centrifuged again. Then, the centrifugation pellet of particles is collected in 1 mL of MilliQ water and lyophilized (Model Lyovax GT2, Steris, Mentor, USA) to obtain a dry powder of $CaCO_3$.

Structural analysis by X-ray diffraction

For some samples, the crystal structures of the obtained $CaCO_3$ particles were characterized by X-ray diffraction (XRD). The XRD analysis was carried out using an X-pert diffractometer (Malvern-PANalytical, UK) using Cu-Kα radiation ($\lambda = 1.54056$ Å) from $2\theta = 10$ to 40° in continuous mode with a step of 0.07°. The crystallite mean sizes were refined using an isotropic Rietveld model with microstrain by means of the MAUD software.[43]

Confocal laser scanning microscopy (CLSM)

All confocal microscopy images were collected with a Leica TCS SP8 AOBS confocal laser scanning microscope (Leica Microsystems, Wetzlar, Germany) equipped with an HC PL APO CS2 63X / NA 1.40 oil objective and gateable hybrid detectors (GaAsP). Images were acquired in 1,024x1,024 pixel format, 8-bit depth, 400 Hz scan speed, and 3X zoom. For the Dextran-FITC used, the excitation was carried out with the 488 nm line of an argon ion laser (40 mW) and the bandpass for the detection of the light emitted was set between 492 and 599 nm. Z-series optical sections were collected with a step size of 0.4 µm using a Super Z Galvo Type H stage and were displayed as maximum z projections or orthogonal projections using LAS software X.

Scanning electron microscopy

To study the morphology and the structure of the $CaCO_3$ microparticles and to determine their diameter, the lyophilized samples were sputtered with gold using a high vacuum metal evaporation coater MED 020 (Bal-Tec, Balzers, Lichtenstein) and observed using a scanning electron microscope (SEM. Jeol 6301F) at an operating voltage of 3 keV. Particle diameters were measured using ImageJ software on multiple images.

For all samples, at least 125 diameters were sampled by measuring all the particles in a representative domain of the picture. For each sample, the average size and distribution standard deviation (SD) were obtained, and 95% confident intervals were computed (assuming a quasi-Gaussian shape of the particle size distribution for the standard deviation, which was a reasonable assumption in view of the monomodal resulting distributions in most cases). Then histograms were built using 0.5 µm width classes in all cases. For comparison convenience, the histograms were plotted as smoothed curves. All these data were normalized so that the area below the curve equals unity.

Results and discussion

Presentation of the process and selection of the parameters

The microfluidic setup used in this study is described in section 2.3. and Fig. 1. Briefly, $scCO_2$ and an aqueous solution of Ca^{2+} are injected via two independent pumps into a micromixer at the entrance of the microfluidic channel. The 0.145 mol/L aqueous Ca^{2+} solution consists of 1.6 wt% of $CaCl_2$ at a pH adjusted to 10. It moreover contains 1 mol/L of glycine to orient the formation of vaterite as previously described in batch conditions.[6] Under these conditions, the initial aqueous solution of calcium remains transparent, and there is no precipitation of $Ca(OH)_2$.[44] It was shown that under similar conditions of concentration, at 40°C and for pressures ranging from 100 to 250 bars, CO_2 dissolves into the aqueous phase when both phases enter into contact, causing a strong decrease of the pH[45] and preventing the formation of $CaCO_3$ particles within the microfluidic channel (data not shown). These conditions of temperature, pressure range, and concentration of Ca^{2+} were therefore selected for the present study. In these conditions, $CaCO_3$ does not form within the microfluidic channel, but only at its end upon depressurization in the pressure regulator. Depressurization indeed causes a decrease of the solubility of CO_2 in the aqueous phase, leading to a pH increase and to the formation of $CaCO_3$ within the aqueous phase at the exit of the microfluidic channel. Since the $scCO_2$ and aqueous phases are not miscible and form a dispersion in the microfluidic channel, a

key question addressed in this study is whether the dispersion state influences the characteristics of the $CaCO_3$ particles obtained at the end of the process. Visualization of the dispersion using the high-speed camera through the sapphire window did not allow identifying the $scCO_2$ and water phases and deducing which one was dispersed and which one was continuous. Still, the efficiency of the dispersion could be evaluated qualitatively by visualizing the size of the droplets observed with the camera. In one extreme case, slugs (Fig. 2a) or very large drops of hundreds of micrometers often reaching the full diameter of the channel (Fig. 2b), are observed, indicating a very poor dispersion efficiency. Intermediary, the slugs/very large droplets are replaced by smaller droplets (Fig. 2c) that decrease in size when the efficiency of the dispersion increases. Ultimately, the dispersion is so efficient that it appears white (highly turbid) to the naked eye and the droplets are so small that they cannot be distinguished with the camera (Fig. 2d). All these dispersion states could be observed by varying the pressure, type of micro-mixer, flow rates of the phases or by adding polymers to the aqueous phase. To discriminate the effect of the dispersion state from other effects, all parameters were investigated separately, and the results were discussed taking into account the dispersion state, qualified using the high-speed camera. The presence of polymer having a significant impact on the dispersion state and on the results, the role of the other parameters is first studied in the absence of polymer

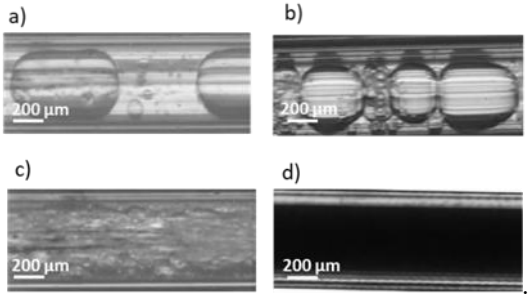

Fig. 2. Representative light microscopy images of the different observed dispersion states within the microfluidic channel no matter the operating conditions. a) slugs; b) extremely large droplets; c) smaller droplets; d) droplets so small that they are not distinguished by the camera (very efficient dispersion). The conditions leading to these different dispersion states are detailed in the different sections, highlighting the role of each parameter (P, flow rates of the phases, type of micromixer, present or absence of added polymer) on this output. Briefly, poor dispersion states (a, b) are favoured in the absence of polymer, with little influence of the other parameters, while the dispersion state is significantly (c), to strongly (d) improved in the presence of amphiphilic block copolymers.

The yield of formation of $CaCO_3$ was estimated at around 60 ± 15% for the different parameters with no systematic impact, precluding any conclusion about the influence of these parameters on the yield. The rather strong variability of the overall carbonation yield was probably due to a poor reproducibility of the recovery yield of the microparticles through successive washing/separation steps. On the contrary, a few experiments were carried out in triplicate with a different experimenter confirming the reproducibility of the results and therefore the robustness of the conclusions regarding the dimensions of the particles (see Appendices, section 2).

1.1. Effect of pressure

Pressure influences the density and viscosity of $scCO_2$ and modifies the interfacial tension between water and $scCO_2$.[40] Changing the pressure may therefore impact the dispersion state of the system. It also affects the solubility of CO_2 in water and consequently the pH, which in turn governs the carbonation. A representative example illustrating the impact of pressure is presented on Fig. 3. It corresponds to a 4 mL/min flow rate of $scCO_2$ mixed with an 8 mL/min flow rate of aqueous calcium solution using a coflow micromixer and without polymer. Changing the pressure from 150 to 250 bar does not affect the dispersion state which remains poor (as presented on Fig. 2a-b). The $CaCO_3$ particles obtained under these conditions are roughly spherical and their diameter is close to 2.4 µm. No significant change of the particle size (Fig. 3a-b) is observed when modifying the pressure. These results suggest that changing the pressure within the 150-250 bar range does not significantly alter the dispersion of both phases nor the morphology or size of the $CaCO_3$ particles. Additional experiments conducted in the absence of polymer with other flow rate conditions further support this conclusion as summarized in Table 1 (details are given in Appendices section 3.1.).

a)

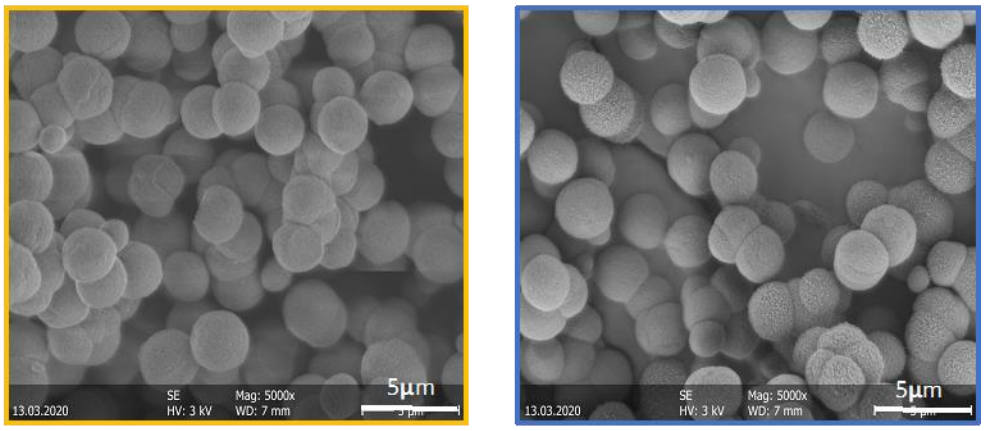

b)

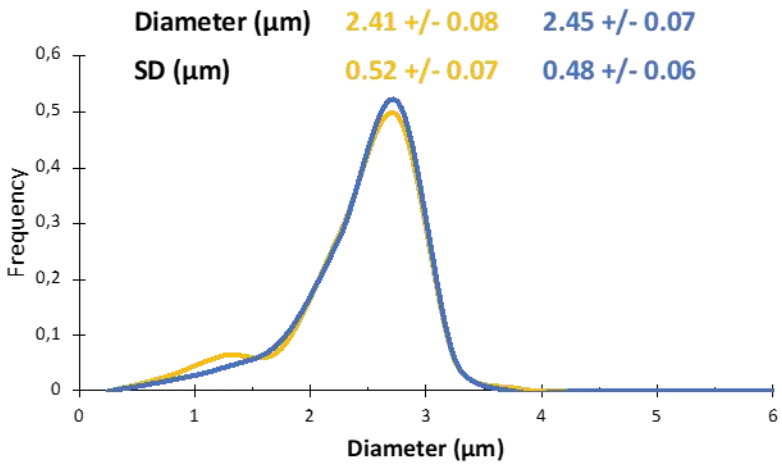

Fig. 3. Impact of pressure on the microfluidic process. Conditions: 40°C, 4 mL/min of $scCO_2$ and 8 mL/min of aqueous calcium chloride solution, coflow micromixer, different pressures, without polymer. Left (yellow): P = 150 bar, Right (blue): P = 250 bar. a) Representative scanning electron microscopy (SEM) images of the $CaCO_3$ particles, b) particle diameter distribution determined from several SEM images.

Table 1. Results of the study of the influence of pressure on the characteristics of particles. Conditions: 40°C, different flow rates, static micromixer, different pressures between 100 and 250 bar, without polymer. ND = Not Determined. In each case, the phases are poorly dispersed, corresponding to Fig. 2a-b.

Rate of flow CO_2sc/Aq phase (mL/min)	Pressure (bar)	Diameter (µm)	Yield (%)
2/1	150	2.9 ± 0.7	ND
	250	2.5 ± 0.6	57
4/8	150	2.4 ± 0.7	ND
	250	2.5 ± 0.4	64
3/3	150	3.7 ± 0.7	ND
	200	3.7 ± 1.0	ND
	250	3.7 ± 1.0	ND

Effect of the flow rates of the $scCO_2$ and aqueous phases

Different flow rate ratios were tested at constant total flow rate, but no systematic effect could be observed precluding any conclusion (see Appendices, section 3.2.). The effect of the total flow rate was then investigated by keeping a constant flow rate ratio of 1 between the aqueous and $scCO_2$ phases. Three different flow rates were selected: 1, 3 and 6 mL/min for each phase. A representative experiment was conducted at P = 250 bar, with a static micromixer and in the absence of polymer. In these conditions, increasing the flow rate of each phase from 1 to 6 mL/min does not improve the efficiency of the dispersion: slugs or very large droplets (Fig. 2a-b) are observed at all flow rates. Fig. 4a and b show that particles obtained at 1 and 3 mL/min are rather large (3-4 µm in diameter) and polydisperse but become significantly smaller (diameter ~1.5 µm) and much more monodisperse at 6 mL/min.

The same conclusions about the impact of the total flow rate were obtained at other pressures (100, 150 and 200 bar) (data not shown) or using a static micromixer instead of a co-flow one (see Appendices, Fig. A7). To summarize, increasing the total flow rate therefore reduces the dimensions and dispersity of the $CaCO_3$ particles. This cannot be due to a variation of the dispersion state which remains constantly poor no matter the flow rate.

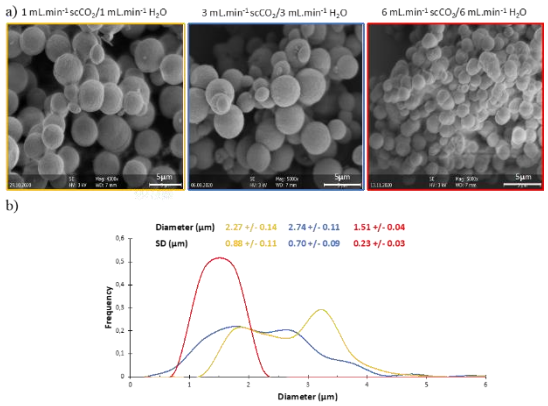

Fig. 4. Impact of the total flow rate on the microfluidic process. Conditions: 40°C, same flow rate for the $scCO_2$ and the aqueous calcium chloride solution, coflow micromixer, P = 250 bar, without polymer. a) Representative scanning electron microscopy (SEM) images of the $CaCO_3$ particles from left to right (yellow, blue, red): 1, 3 and 6 mL/min for each phase, b) particle diameter distribution determined from several SEM images: 1-, 3 - and 6 - mL/min for each phase.

Effect of the micromixer type

The conditions of flow rates used for the coflow micromixer were also applied to a static micromixer with the objective to change the dispersion state without changing the flow rate and investigate the consequences on the characteristics of the $CaCO_3$ particles (Fig. 5). In spite of its specific design allowing strong mixing of the two phases at the entrance of the microfluidic channel and local

turbulent flow inside the porous frit of the static micromixer, the static micromixer is not sufficient to achieve a more efficient dispersion of both phases: slugs or very large droplets (Fig. 2a-b) are also observed with the co-flow micromixer in the absence of polymer (no matter P or the flow rates). Fig. 5 indicates that there is no significant difference in terms of particle sizes between the two types of micromixers. As a conclusion, in the absence of polymer, the type of micromixer does not influence the dispersion state, nor the dimensions of the $CaCO_3$ particles.

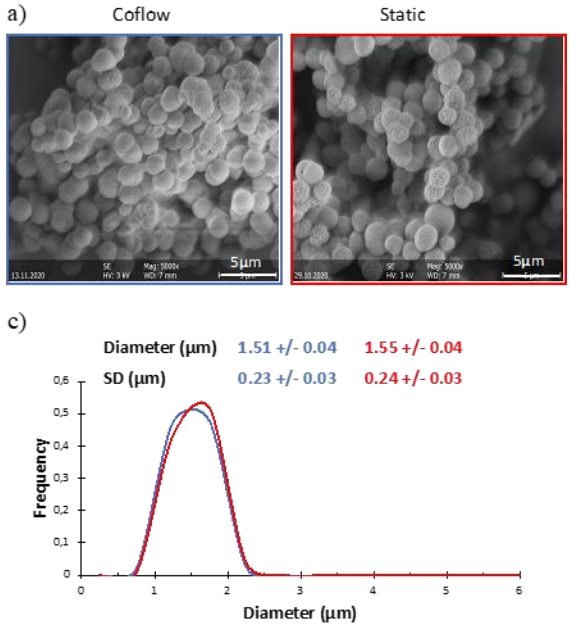

Fig. 5. Impact of the type of micromixer. Conditions: 40°C, 6 mL/min of $scCO_2$ and 6 mL/min of aqueous calcium chloride solution, P = 250 bar, different micromixers: Left (blue): coflow micromixer, Right (red): static micromixer. a) Representative scanning electron microscopy (SEM) images of the $CaCO_3$ particles, b) particle diameter distribution determined from several SEM images.

Effect of polymer addition

In the absence of polymer, changing the pressure, the flow rate or the type of micromixer did not affect the dispersion state of both phases within the microchannel which always remained poor (Fig. 2a-b). A slight decrease of the size of the particles was observed at high flow rate (6 mL/min) with both micromixers, but it was not correlated to a change of the dispersion state. The effect of the dispersion state on the dimensions of the $CaCO_3$ particles could actually not be inferred from the previous experiments. To improve the dispersion state of phases and evaluate the effect of this parameter, two amphiphilic copolymers were used at a concentration of 1 wt% in the aqueous phase. The first copolymer is a poly(dimethyl siloxane)-*block*-poly(oligoethyleneglycol methacrylate) exhibiting degrees of polymerization (DP_n) of 13 and 46 respectively for the first and second block ($PDMS_{13}$-*b*-$POEGMA_{46}$). The synthesis of this polymer, its ability to decrease strongly the $scCO_2$/water interfacial tension and to stabilize $scCO_2$/water emulsions were previously reported.[40] The other amphiphilic copolymer is a commercial poly(ethylene oxide)-*block*-poly(propylene oxide)-block-poly(ethylene oxyde) triblock copolymer (Pluronic® PE 6400) with DP_n = 13, 30 and 13 respectively for its three blocks (PEO_{13}-PPO_{30}-PEO_{13}).[46] PEO_{13}-PPO_{30}-PEO_{13} has also the ability to decrease strongly the $scCO_2$-water interfacial tension and to stabilize $scCO_2$/water emulsions (see Appendices, section 3.3.1.).

The addition of polymer has a strong effect compared to the same conditions in the absence of polymer. First, the presence of $PDMS_{13}$-*b*-$POEGMA_{46}$ or PEO_{13}-PPO_{30}-PEO_{13} strongly improves the dispersion state of the $scCO_2$ and aqueous phases: at sufficiently large total flow rates (≥ 3 mL/min), slugs/large droplets (Fig. 2a-b) eventually transform into much smaller droplets of each phase (typically a few tens of microns, see Fig. 2c, or even so small that they cannot be distinguished leading to an opaque dispersion, Fig. 2d – details in Appendices, Section 3.3.2.). This observation is true no matter the pressure, the flow rate, or the type of micromixer although the dimensions of the droplets (quality of dispersion) vary depending on these parameters. The most efficient dispersions are obtained at 6 mL/min of each phase and with the static micromixer, leading to droplets so small that they cannot be distinguished with the digital camera (Fig. 2d, details in Appendices, Section 3.3.2.). The improvement of the dispersion state in the presence of these polymers was expected considering that they are amphiphilic. Indeed, first they decrease the water-$scCO_2$ interfacial tension, thereby favoring the formation of smaller dispersed droplets. Moreover, they are able to stabilize the obtained droplets as mentioned above.

Besides, a strong decrease of the dimensions of the $CaCO_3$ particles is observed in the presence of the amphiphilic copolymers compared to the same conditions in the absence of copolymer. This can be seen for example on Fig. 6 for a representative case (coflow micromixer, 250 bar, 4 mL/min of $scCO_2$ and 8 mL/min of aqueous calcium chloride solution – compare the data for $PDMS_{13}$-*b*-$POEGMA_{46}$ or PEO_{13}-PPO_{30}-PEO_{13} with those in the absence of polymer). Additional experiments conducted with other flow rate and pressure conditions or with

$PDMS_{13}$-*b*-$POEGMA_x$ with shorter POEGMA blocks (x = 16 or 31) confirmed these conclusions (Table 3 and additional experiments in Appendices, section 3.3.2.).

It would be tempting here to conclude that a correlation exists between the improvement of the dispersion and the decrease of the size of the $CaCO_3$ particles. However, blank experiments were conducted with hydrophilic homopolymers (at 1 wt% in the water phase): Dextran 40 kg/mol, Dextran 500 kg/mol (Fig. 6) and $POEGMA_{31}$ (see Appendices, section 3.3.2.). These polymers do not favour the dispersion of the phases (slugs are observed as in the absence of polymer – Fig. 6a). Still, Fig. 6c and Table 3 clearly indicate that the dimensions of the $CaCO_3$ particles are also reduced with these hydrophilic homopolymers compared to the polymer-free aqueous solutions. The diameter of the $CaCO_3$ particles is even the same with Dextran 40 kg/mol as with the amphiphilic copolymers. These results undoubtedly imply that there is absolutely no correlation between the efficiency of the $scCO_2$/aqueous phase dispersion and the diameter of the final $CaCO_3$ particles (additional data confirming this conclusion are presented in the Appendices, section 3.3.2.).

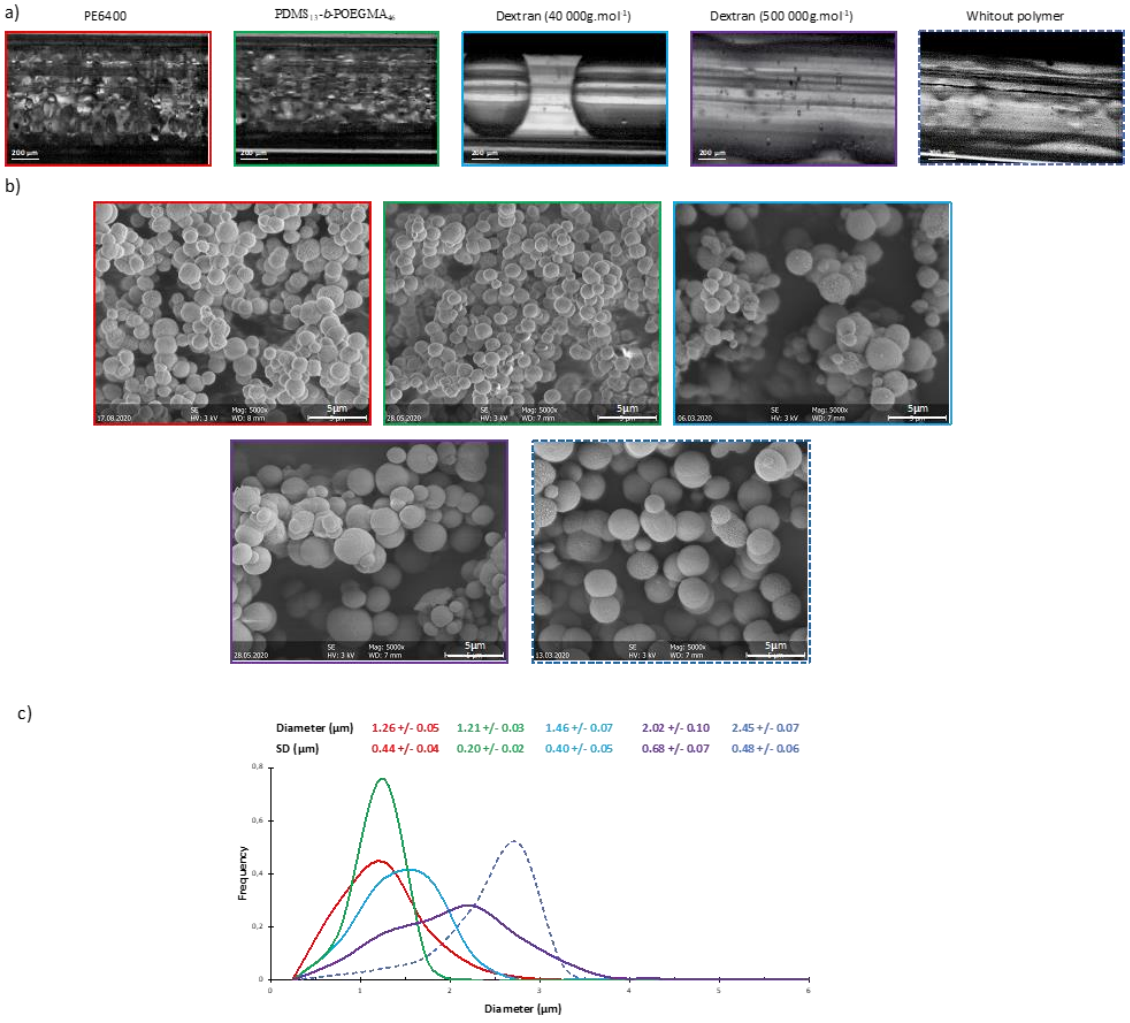

Fig. 6. Impact of the presence of polymer. Conditions: 40°C, 4 mL/min of $scCO_2$ and 8 mL/min of aqueous calcium chloride solution, coflow micromixer, P = 250 bar, with 1 wt% of different polymers in the aqueous phase: PEO_{13}-PPO_{30}-PEO_{13} (PE6400) —, $PDMS_{13}$-b-$POEGMA_{46}$ —, Dextran (40,000 g/mol) —; Dextran (500,000 g/mol) — or without polymer (-- -). a) Optical images of the dispersion within the microfluidic channel, b) representative scanning electron microscopy (SEM) images of the $CaCO_3$ particles, c) particle diameter distribution determined from several SEM images.

Note that in the presence of polymer, neither the pressure (in the range 150-250 bar) nor the type of micromixer (coflow or static micromixer) affect the diameter of the $CaCO_3$ particles (Tables 2, A2 and A3), their structure or morphology, keeping other parameters constant. On the contrary, increasing the flow rate from 1 to 6 mL/min for both phases significantly decreases the average diameter and width of the particles distribution (see Appendices, section 3.3.2.). These conclusions are qualitatively the same as those reached in the absence of polymer.

Table 2. Results of the study of the influence of polymers and pressure on the particle and crystallite sizes determined by XRD. Conditions: 40°C, Flowrates: 4 mL/min $scCO_2$ / 8 mL/min aqueous solution of calcium chloride, Coflow micromixer, 100 and 250 bar, without or with polymer (1 wt% in the aqueous phase). ND = Not Determined.

Pressure	Polymers	Particle diameter (μm)	Crystallite size (nm)	Yield (%)
150 bar	**Without polymer**	**2.4 ± 0.5**	**43.4 ± 0.8**	**ND**
	$PDMS_{13}$-*b*-$POEGMA_{46}$	1.6 ± 0.3	38.8 ± 0.7	61
	PEO_{13}-PPO_{30}-PEO_{13}	1.2 ± 0.4	35.4 ± 0.6	67
	Dextran (40 000 $g.mol^{-1}$)	1.9 ± 0.3	42.7 ± 0.8	ND
250 bar	**Without polymer**	**2.5 ± 0.5**	**39.5 ± 0.8**	**64**
	$PDMS_{13}$-*b*-$POEGMA_{46}$	1.2 ± 0.2	38.2 ± 0.7	ND
	PEO_{13}-PPO_{30}-PEO_{13}	1.2 ± 0.4	39.4 ± 0.6	77
	Dextran (40 000 $g.mol^{-1}$)	1.5 ± 0.4	39.3 ± 0.5	ND

Elucidation of the role of the different parameters
Role of the polymer on the structure of the precipitated $CaCO_3$ particles

The results presented above lead to the conclusion that no matter the pressure, the phases flow rate, the type of micromixer and whether a polymer is added or not into the formulation, spherical vaterite $CaCO_3$ particles exhibiting diameters in the micrometer range can be obtained with a continuous microfluidic process involving a dispersion of $scCO_2$ and aqueous calcium solution. A conclusion which may appear surprising in view of the literature on carbonation processes in microemulsions mentioned in the introduction is that there was no correlation between the dispersion state of the $scCO_2$-aqueous phases and the diameter of the particles. It was not possible to determine which phase was the dispersed one, making it impossible to know if the particles are formed in the droplets or in the continuous phase. However, compared to the carbonation in microemulsions,[16,47] the dispersed droplets obtained in this study were always actually quite large (tens to hundreds of microns) compared to those of the $CaCO_3$ particles (a few microns). This probably explains why better dispersion states (smaller droplets of each phase) did not impact the dimensions of the $CaCO_3$ particles in our study.

Two parameters had an influence on the particles: the diameter of the $CaCO_3$ particles could be divided by a factor of ~2 (which represents an increase by a factor 4 in terms of surface area and can be very significant for many applications) by increasing the flow rate and/or by adding a neutral polymer to the aqueous phase.

To understand these results, the $CaCO_3$ particles were investigated in more details by X-Ray diffraction. It was indeed previously reported that crystallization of $CaCO_3$ in the presence of glycine resulted in the formation of small nanocrystals[19,41,42] of vaterite with dimensions in the tens of nanometers range which then aggregated into large spherical and microporous clusters.[2] X-Ray diffraction allows determining the diameter of the vaterite nanocrystals in addition to confirming the vaterite polymorphic structure. Fig. 7 and Table 3 confirm on a few representative examples that pure vaterite is obtained in all cases. Moreover, the width of the diffraction peaks is nearly identical in all conditions. It indicates that the size of the individual aggregated nanocrystallites (~40 nm) forming the vaterite microspheres is not affected either by the type of polymer nor by the flow rate of the phases.

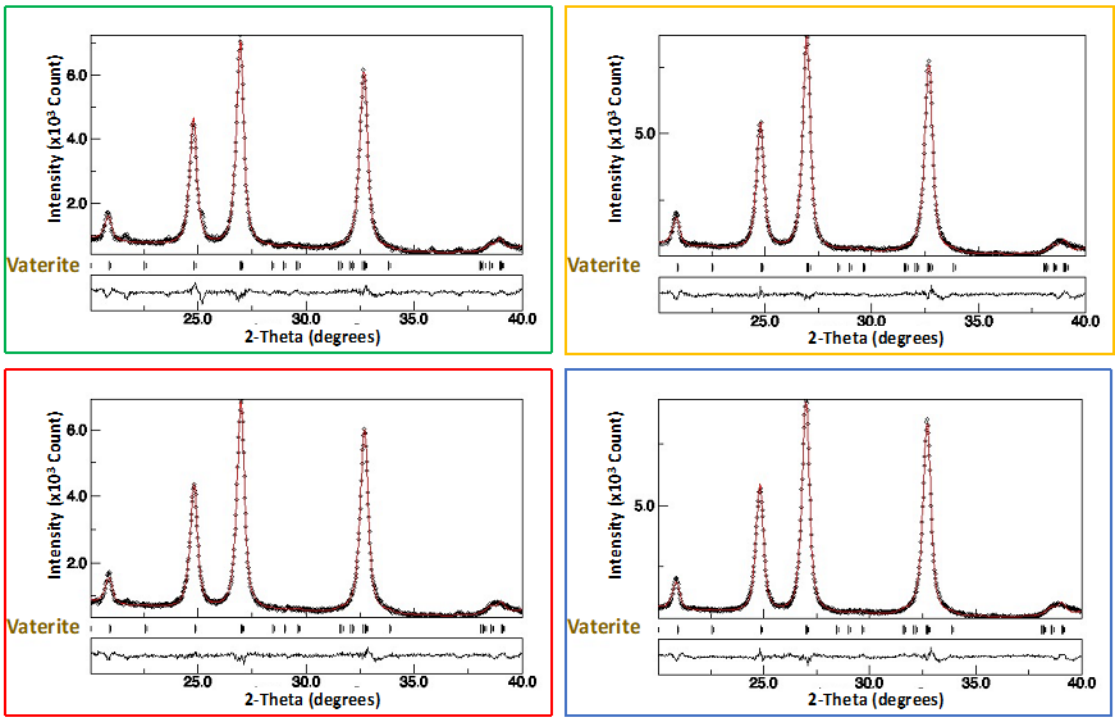

Fig. 7. Representative X-ray diffractograms of the vaterite $CaCO_3$ microspheres at 4 mL/min $scCO_2$ / 8 mL/min aqueous solution of calcium chloride at 250 bar, coflow micromixer, 40°C, 1 wt% of polymer in the aqueous phase with different polymers: PEO_{13}-PPO_{30}-PEO_{13} —, $PDMS_{13}$-b-$POEGMA_{46}$ —, Dextran (40,000 g/mol) — and without polymer —. Bragg reflexions of vaterite (ICSD 15879) are indicated with vertical markers below the profile.

Now in the presence of polymer, all other conditions being constant, the diameter of the final $CaCO_3$ particles decreases no matter whether the polymer is hydrophilic or amphiphilic. Importantly, this happens although neither the carbonation yield nor the polymorphism, morphology or dimensions of the individual crystallites aggregating into vaterite microspheres (~40 nm) are affected. It follows that the particles formed in the presence of polymer result from the aggregation of fewer crystallites. Since the only difference is the presence of the polymer, the dispersion state playing no role, the polymer probably interacts with the crystallites and limit their aggregation, and consequently the particle size.

Many polymers have been reported in the literature as additives altering the characteristics of $CaCO_3$ particles, mainly their polymorphism.[48,49] However, almost all these polymers were polyelectrolytes strongly interacting with Ca^{2+} and/or CO_3^{2-} ions, which explains their impact on the crystallization process. Hardikar et al.[50] used cationic, anionic or neutral dextran during the crystallization of $CaCO_3$ and observed that the charged polymers strongly affected the characteristics of the $CaCO_3$ particles, whereas neutral dextran had no significant impact. They concluded that neutral dextran did not interact with $CaCO_3$ during its formation, which somehow contradicts our assumptions. In order to check our hypothesis, fluorescein-labelled dextran (Dextran-FITC 40kg/mol) was used to prepare $CaCO_3$ particles. Confocal microscopic observations in Fig. 8 revealed that the resulting $CaCO_3$ particles fluoresced at the wavelength of excitation of fluorescein, indicating that labelled-dextran was part of the particles and homogeneously distributed in their porous structure.

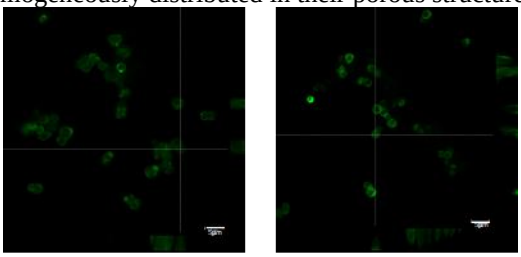

Fig. 8. Confocal laser scanning microscopy images of the $CaCO_3$ particles obtained in the presence of 1 wt% Dextran-FITC 40 kg/mol. Conditions: 40°C, 4 mL/min of $scCO_2$ and 8 mL/min of aqueous calcium chloride solution, P = 250 bar, coflow micromixer.

This confirms that this polymer interacts with $CaCO_3$ and probably affects the aggregation of the crystallites. Two mechanisms could explain this phenomenon.

Firstly, the presence of polymer could lead to the formation of more nuclei, which would increase the number of particles, leading to a decrease of the number of crystallites per particles (hence decreasing their diameter). Secondly, polymers could prevent the crystallite aggregation and thus limit the particle diameter. Most probably, a combination of these two phenomena happens (Fig. 9). EDX analysis by SEM of $CaCO_3$ particles prepared in the presence of $PDMS_{13}$-*b*-$POEGM_{31}$ also revealed a strong concentration of silicon (indicative of the presence of the polymer) on/in the $CaCO_3$ particles, confirming the results obtained with dextran-FITC (see Appendices, section 3.4.). This technique does not allow determining whether the polymer is located within the $CaCO_3$ particles or on their surface, since EDX probes the sample at the micron scale, which roughly corresponds to the dimensions of the particles. The polymer-$CaCO_3$ interaction is however weak in our case since only a moderate decrease (factor 2) of the diameter of the particles is observed, whereas completely different morphologies and crystalline structures were observed by Hardikar et al. using charged dextrans. This explains the conclusions of these authors compared to ours.

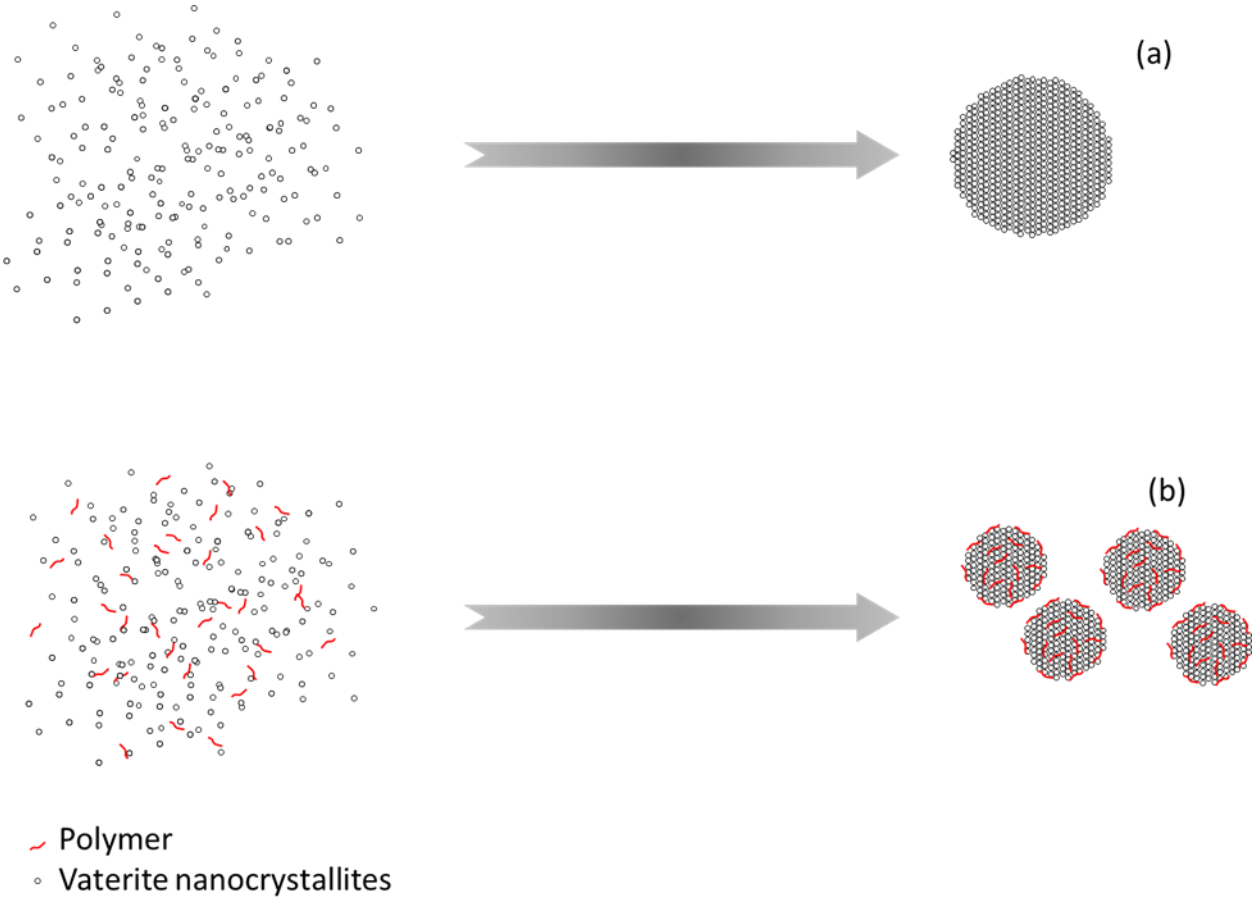

Fig. 9. Proposed mechanism for the nanostructured $CaCO_3$ particle formation (a) in absence and (b) in the presence of polymer: the polymer chains probably act as nuclei for the aggregation of the primary $CaCO_3$ crystallites (~ 40 nm) and/or limit the aggregation of the crystallites, both phenomena leading to smaller $CaCO_3$ vaterite particles compared to what is obtained in the absence of polymer.

Key role of depressurization

Changing the flow rate does not add anything to the reaction medium. The role of the flow rate can therefore not be explained in the same way as the role of the polymer. It can certainly not be explained by a modification of the dispersion state either, since this latter parameter is not correlated to the dimensions of the particles. To understand the role of the flow rate, it must be kept in mind that the formation of $CaCO_3$ particles only occurs at the end of the microfluidic channel upon depressurization. Depressurization, which occurs within the pressure valve placed at the end of the channel, indeed causes a decrease of P, leading to an increase of pH and allowing $CaCO_3$ to become stable (see section 3.1). Increasing the flow rate within the channel necessarily reduces the residence time of the aqueous solution in this valve and therefore increases the depressurization rate. This leads to a faster desorption of CO_2 from the aqueous phase, accompanied by a faster pH-modification and therefore a faster $CaCO_3$ crystallization. Still, the individual nanocrystallites have roughly the same size. Then, to cope with the faster depressurization at higher flow rates, the nanocrystallites probably form more nuclei, resulting in a higher number of smaller particles in the end.

This would mean that the actual parameter being changed upon variation of the flow rate is the depressurization speed. To check that this variable indeed affects the characteristics of the particles, the microfluidic process was compared to a batch process keeping constant the composition of these phases (Fig. 10).

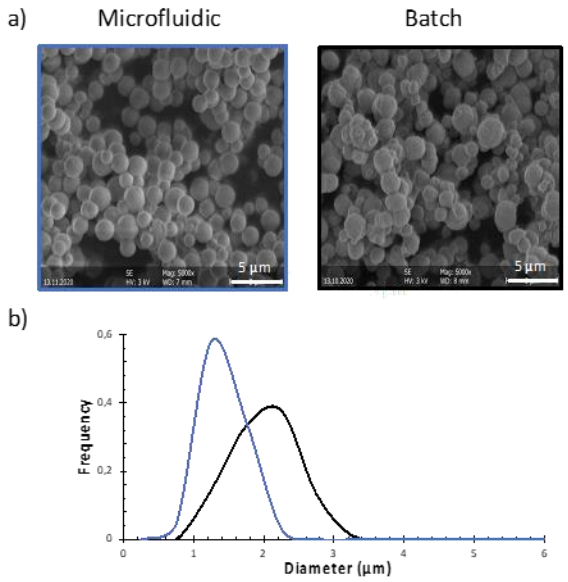

Fig. 10. Impact of the depressurization conditions on the characteristics of the $CaCO_3$ particles. Conditions: 40°C, P = 250 bar, with 1 wt% of PEO_{13}-PPO_{30}-PEO_{13} in the aqueous phase. a) Representative scanning electron microscopy (SEM) images of the $CaCO_3$ and b) particle diameter distributions determined from several SEM images Batch process (volume phase ratio $scCO_2$ / aqueous solution is 19/1) — and Microfluidic process (at 6 mL/min $scCO_2$ / 6 mL/min aqueous solution of calcium chloride)—.

The $CaCO_3$ particles obtained with the batch process exhibit larger dimensions and dispersity than those formed with the microfluidic process. The depressurization takes a few minutes using a manual depressurization valve for the batch process, whereas it occurs in a fraction of a second at the end of the microfluidic channel. It is therefore confirmed that the depressurization speed affects the dimensions of the particles. Investigating what happens in the depressurization valve seems necessary to better understand the process. This could be achieved for example by using a depressurization valve allowing control of the depressurization speed and residence time. However, this represents a study in itself which falls out of the scope of the present paper.

Conclusion

A microfluidic high pressure experimental setup enabled the continuous production of microparticles of calcium carbonate by mixing a Ca^{2+} aqueous phase and supercritical CO_2 as a carbonate source. This work aimed at characterizing the effect of different process and formulation parameters on the water-$scCO_2$ dispersion efficiency and on the properties of the obtained microparticles including their size, polydispersity, and polymorphism.

Independently of the process and formulation conditions, all the obtained $CaCO_3$ particles are composed of self-assembled vaterite nanocrystallites of about 40 nm (confirmed by DRX) which aggregate into micrometric spheres with a carbonation yield of around 60%. These particles have the same size of nanocrystallites and the same spherical structure as the particles already obtained previously,[2,19] so their porosity can also be considered identical. Varying the pressure within the microfluidic channel or the type of micromixer has no effect on the size of the $CaCO_3$

microparticles. On the contrary, adding a polymer into the aqueous phase or increasing the flow rate of each phase to 6 mL/min decreased the diameter of the particles by a factor two.

It was proven by using polymers affecting differently the dispersion state of the phases within the microfluidic channel that the dimensions of the particles are not affected by the dimensions of the droplets within the dispersions. This result is relevant since it seems to contradict the carbonation studies in microemulsion which showed that the dimensions of the particles are correlated to some extent with that of the microemulsion domains. However, in this work, the droplets within the microfluidic channel are much larger (tens to hundreds of micrometers) than the $CaCO_3$ particles (a few microns). Moreover, the particles are actually not formed within the microfluidic channel but at its end, upon depressurization. This probably explains the strong differences with the carbonation studies in microemulsion.

The impact of the polymer was attributed to its ability to interact with the nanocrystallites during the precipitation step, thereby leading to smaller and less polydisperse $CaCO_3$ particles obtained in the presence of the polymer. The impact of the flow rate was not correlated to the dispersion state and was associated to the rate of depressurization at the end of the microfluidic channel: higher flow rates increased the speed of CO_2 desorption from the aqueous phase, causing a faster precipitation and leading to more numerous but smaller $CaCO_3$ particles.

The present work shows promising results of the high scalability and robustness of this continuous carbonation process for the elaboration of well nanostructured vaterite microparticles with controlled size for drug delivery applications.

Acknowledgements

This work was supported by the Region Pays de Loire (France) in the frame of the SPEED program (Ph.D. grant to P. Legout). The authors thank the SCIAM laboratory (Angers, France) for SEM analysis.

References

(1) Mattila, H.-P.; Zevenhoven, R. Production of Precipitated Calcium Carbonate from Steel Converter Slag and Other Calcium-Containing Industrial Wastes and Residues. In *Advances in Inorganic Chemistry*; Elsevier, 2014; Vol. 66, pp 347–384. https://doi.org/10.1016/B978-0-12-420221-4.00010-X.

(2) Chavez Panduro, E. A.; Beuvier, T.; Fernández Martínez, M.; Hassani, L.; Calvignac, B.; Boury, F.; Gibaud, A. Small-Angle X-Ray Scattering Analysis of Porous Powders of $CaCO_3$. *J. Appl. Crystallogr.* **2012**, *45* (5), 881–889. https://doi.org/10.1107/S0021889812032219.

(3) Ferreira, A. M.; Vikulina, A. S.; Volodkin, D. CaCO3 Crystals as Versatile Carriers for Controlled Delivery of Antimicrobials. *J. Controlled Release* **2020**, *328*, 470–489. https://doi.org/10.1016/j.jconrel.2020.08.061.

(4) Tran, M.-K.; Hassani, L. N.; Calvignac, B.; Beuvier, T.; Hindré, F.; Boury, F. Lysozyme Encapsulation within PLGA and CaCO3 Microparticles Using Supercritical CO2 Medium. *J. Supercrit. Fluids* **2013**, *79*, 159–169. https://doi.org/10.1016/j.supflu.2013.02.024.

(5) Zhan, J.; Lin, H.-P.; Mou, C.-Y. Biomimetic Formation of Porous Single-Crystalline CaCO3 via Nanocrystal Aggregation. *Adv. Mater.* **2003**, *15* (78), 621–623. https://doi.org/10.1002/adma.200304600.

(6) Hassani, L. N.; Hindré, F.; Beuvier, T.; Calvignac, B.; Lautram, N.; Gibaud, A.; Boury, F. Lysozyme Encapsulation into Nanostructured CaCO3 Microparticles Using a Supercritical CO2 Process and Comparison with the Normal Route. *J. Mater. Chem. B* **2013**, *1* (32), 4011. https://doi.org/10.1039/c3tb20467g.

(7) Vikulina, A.; Webster, J.; Voronin, D.; Ivanov, E.; Fakhrullin, R.; Vinokurov, V.; Volodkin, D. Mesoporous Additive-Free Vaterite CaCO3 Crystals of Untypical Sizes: From Submicron to Giant. *Mater. Des.* **2021**, *197*, 109220. https://doi.org/10.1016/j.matdes.2020.109220.

(8) Pascual, C. D.; Subra-Paternault, P. *Supercritical Fluid Nanotechnology: Advances and Applications in Composites and Hybrid Nanomaterials*, 0 ed.; Jenny Stanford Publishing, 2015. https://doi.org/10.1201/b19242.

(9) Hirai, T.; Hariguchi, S.; Komasawa, I.; Davey, R. J. Biomimetic Synthesis of Calcium Carbonate Particles in a Pseudovesicular Double Emulsion. *Langmuir* **1997**, *13* (25), 6650–6653. https://doi.org/10.1021/la9705266.

(10) Fujiwara, M.; Shiokawa, K.; Araki, M.; Ashitaka, N.; Morigaki, K.; Kubota, T.; Nakahara, Y. Encapsulation of Proteins into $CaCO_3$ by Phase

Transition from Vaterite to Calcite. *Cryst. Growth Des.* **2010**, *10* (9), 4030–4037. https://doi.org/10.1021/cg100631v.
(11) Tai, C. Y.; Chen, C. Particle Morphology, Habit, and Size Control of CaCO3 Using Reverse Microemulsion Technique. *Chem. Eng. Sci.* **2008**, *63* (14), 3632–3642. https://doi.org/10.1016/j.ces.2008.04.022.
(12) Viravaidya, C.; Li, M.; Mann, S. Microemulsion-Based Synthesis of Stacked Calcium Carbonate (Calcite) Superstructures. *Chem. Commun.* **2004**, No. 19, 2182. https://doi.org/10.1039/b408041f.
(13) Rock, M. L.; Tranchitella, L. J.; Pilato, R. S. Control of Calcium Carbonate Particle Size and Shape by Precipitation from CTAB/Alcohol/Hexadecane Mixtures. *Colloid Polym. Sci.* **1997**, *275* (9), 893–896. https://doi.org/10.1007/s003960050163.
(14) Rauscher, F.; Veit, P.; Sundmacher, K. Analysis of a Technical-Grade w/o-Microemulsion and Its Application for the Precipitation of Calcium Carbonate Nanoparticles. *Colloids Surf. Physicochem. Eng. Asp.* **2005**, *254* (1–3), 183–191. https://doi.org/10.1016/j.colsurfa.2004.11.034.
(15) Kang, S. H.; Hirasawa, I.; Kim, W.-S.; Choi, C. K. Morphological Control of Calcium Carbonate Crystallized in Reverse Micelle System with Anionic Surfactants SDS and AOT. *J. Colloid Interface Sci.* **2005**, *288* (2), 496–502. https://doi.org/10.1016/j.jcis.2005.03.015.
(16) Kandori, K.; Kon-no, K.; Kitahara, A. Formation of Ionic Water/Oil Microemulsions and Their Application in the Preparation of CaCO3 Particles. *J. Colloid Interface Sci.* **1988**, *122* (1), 78–82. https://doi.org/10.1016/0021-9797(88)90289-5.
(17) Bandyopadhyaya, R.; Kumar, R.; Gandhi, K. S.; Ramkrishna, D. Modeling of Precipitation in Reverse Micellar Systems. *Langmuir* **1997**, *13* (14), 3610–3620. https://doi.org/10.1021/la960599+.
(18) Anbu, P.; Kang, C.-H.; Shin, Y.-J.; So, J.-S. Formations of Calcium Carbonate Minerals by Bacteria and Its Multiple Applications. *SpringerPlus* **2016**, *5* (1), 250. https://doi.org/10.1186/s40064-016-1869-2.
(19) Beuvier, T.; Calvignac, B.; Delcroix, G. J.-R.; Tran, M. K.; Kodjikian, S.; Delorme, N.; Bardeau, J.-F.; Gibaud, A.; Boury, F. Synthesis of Hollow Vaterite CaCO3 Microspheres in Supercritical Carbon Dioxide Medium. *J. Mater. Chem.* **2011**, *21* (26), 9757. https://doi.org/10.1039/c1jm10770d.
(20) Domingo, C.; García-Carmona, J.; Loste, E.; Fanovich, A.; Fraile, J.; Gómez-Morales, J. Control of Calcium Carbonate Morphology by Precipitation in Compressed and Supercritical Carbon Dioxide Media. *J. Cryst. Growth* **2004**, *271* (1–2), 268–273. https://doi.org/10.1016/j.jcrysgro.2004.07.060.
(21) Domingo, C.; Loste, E.; Gómez-Morales, J.; García-Carmona, J.; Fraile, J. Calcite Precipitation by a High-Pressure CO2 Carbonation Route. *J. Supercrit. Fluids* **2006**, *36* (3), 202–215. https://doi.org/10.1016/j.supflu.2005.06.006.
(22) Beuvier, T.; Calvignac, B.; Delcroix, G. J.-R.; Tran, M. K.; Kodjikian, S.; Delorme, N.; Bardeau, J.-F.; Gibaud, A.; Boury, F. Synthesis of Hollow Vaterite CaCO3 Microspheres in Supercritical Carbon Dioxide Medium. *J. Mater. Chem.* **2011**, *21* (26), 9757. https://doi.org/10.1039/c1jm10770d.
(23) Boury, F.; Benoit, J.-P.; Tewes, F.; Thomas, O. Method for Preparing Particles from an Emulsion in Supercritical or Liquid CO2. WO2007072106A1, 2005.
(24) Niculescu, A.-G.; Chircov, C.; Bîrcă, A. C.; Grumezescu, A. M. Nanomaterials Synthesis through Microfluidic Methods: An Updated Overview. *Nanomaterials* **2021**, *11* (4), 864. https://doi.org/10.3390/nano11040864.
(25) Trushina, D. B.; Bukreeva, T. V.; Kovalchuk, M. V.; Antipina, M. N. CaCO3 Vaterite Microparticles for Biomedical and Personal Care Applications. *Mater. Sci. Eng. C* **2014**, *45*, 644–658. https://doi.org/10.1016/j.msec.2014.04.050.
(26) Zeynep, E. Y.; Antoine, D.; Brice, C.; Frank, B.; Christine, J. Double Hydrophilic Polyphosphoester Containing Copolymers as Efficient Templating Agents for Calcium Carbonate Microparticles. *J. Mater. Chem. B* **2015**, *3* (36), 7227–7236. https://doi.org/10.1039/C5TB00887E.
(27) Yashina, A.; Meldrum, F.; deMello, A. Calcium Carbonate Polymorph Control Using Droplet-Based Microfluidics. *Biomicrofluidics* **2012**, *6* (2), 022001. https://doi.org/10.1063/1.3683162.
(28) Svenskaya, Y. I.; Fattah, H.; Inozemtseva, O. A.; Ivanova, A. G.; Shtykov, S. N.; Gorin, D. A.; Parakhonskiy, B. V. Key Parameters for Size- and Shape-Controlled Synthesis of Vaterite Particles. *Cryst. Growth Des.* **2018**, *18* (1), 331–337. https://doi.org/10.1021/acs.cgd.7b01328.
(29) Liu, P.; Yao, J.; Couples, G. D.; Ma, J.; Iliev, O. 3-D Modelling and Experimental Comparison of Reactive Flow in Carbonates under Radial Flow Conditions. *Sci. Rep.* **2017**, *7* (1), 17711. https://doi.org/10.1038/s41598-017-18095-2.
(30) Li, S.; Ihli, J.; Marchant, W. J.; Zeng, M.; Chen, L.; Wehbe, K.; Cinque, G.; Cespedes, O.; Kapur, N.; Meldrum, F. C. Synchrotron FTIR Mapping of Mineralization in a Microfluidic Device. *Lab. Chip* **2017**, *17* (9), 1616–1624. https://doi.org/10.1039/C6LC01393G.
(31) Luther, S. K.; Braeuer, A. High-Pressure Microfluidics for the Investigation into Multi-Phase Systems Using the Supercritical Fluid Extraction of Emulsions (SFEE). *J. Supercrit. Fluids* **2012**, *65*, 78–86. https://doi.org/10.1016/j.supflu.2012.02.029.

(32) Giroire, B.; Marre, S.; Garcia, A.; Cardinal, T.; Aymonier, C. Continuous Supercritical Route for Quantum-Confined GaN Nanoparticles. *React. Chem. Eng.* **2016**, *1* (2), 151–155. https://doi.org/10.1039/C5RE00039D.
(33) Jaouhari, T.; Zhang, F.; Tassaing, T.; Fery-Forgues, S.; Aymonier, C.; Marre, S.; Erriguible, A. Process Intensification for the Synthesis of Ultra-Small Organic Nanoparticles with Supercritical CO2 in a Microfluidic System. *Chem. Eng. J.* **2020**, *397*, 125333. https://doi.org/10.1016/j.cej.2020.125333.
(34) Daro, N.; Vaudel, T.; Afindouli, L.; Marre, S.; Aymonier, C.; Chastanet, G. One-Step Synthesis of Spin Crossover Nanoparticles Using Flow Chemistry and Supercritical CO_2. *Chem. – Eur. J.* **2020**, *26* (69), 16286–16290. https://doi.org/10.1002/chem.202002322.
(35) Jaouhari, T.; Marre, S.; Tassaing, T.; Fery-Forgues, S.; Aymonier, C.; Erriguible, A. Investigating Nucleation and Growth Phenomena in Microfluidic Supercritical Antisolvent Process by Coupling in Situ Fluorescence Spectroscopy and Direct Numerical Simulation. *Chem. Eng. Sci.* **2022**, *248*, 117240. https://doi.org/10.1016/j.ces.2021.117240.
(36) Kang, S. H.; Hirasawa, I.; Kim, W.-S.; Choi, C. K. Morphological Control of Calcium Carbonate Crystallized in Reverse Micelle System with Anionic Surfactants SDS and AOT. *J. Colloid Interface Sci.* **2005**, *288* (2), 496–502. https://doi.org/10.1016/j.jcis.2005.03.015.
(37) Zhang, F.; Marre, S.; Erriguible, A. Mixing Intensification under Turbulent Conditions in a High Pressure Microreactor. *Chem. Eng. J.* **2020**, *382*, 122859. https://doi.org/10.1016/j.cej.2019.122859.
(38) Zhang, F.; Erriguible, A.; Marre, S. Investigating Laminar Mixing in High Pressure Microfluidic Systems. *Chem. Eng. Sci.* **2019**, *205*, 25–35. https://doi.org/10.1016/j.ces.2019.03.063.
(39) Marre, S.; Aymonier, C.; Subra, P.; Mignard, E. Dripping to Jetting Transitions Observed from Supercritical Fluid in Liquid Microcoflows. *Appl. Phys. Lett.* **2009**, *95* (13), 134105. https://doi.org/10.1063/1.3242375.
(40) Legout, P.; Lefebvre, G.; Bonnin, M.; Gimel, J.-C.; Benyahia, L.; Colombani, O.; Calvignac, B. Synthesis of PDMS- *b* -POEGMA Diblock Copolymers and Their Application for the Thermoresponsive Stabilization of Water-Supercritical Carbon Dioxide Emulsions. *Langmuir* **2020**, *36* (43), 12922–12932. https://doi.org/10.1021/acs.langmuir.0c02194.
(41) Hou, W.; Feng, Q. A Simple Method to Control the Polymorphs of Calcium Carbonate in CO2-Diffusion Precipitation. *J. Cryst. Growth* **2005**, *282* (1–2), 214–219. https://doi.org/10.1016/j.jcrysgro.2005.04.102.
(42) Shivkumara, C.; Singh, P.; Gupta, A.; Hegde, M. S. Synthesis of Vaterite CaCO3 by Direct Precipitation Using Glycine and L-Alanine as Directing Agents. *Mater. Res. Bull.* **2006**, *41* (8), 1455–1460. https://doi.org/10.1016/j.materresbull.2006.01.026.
(43) *Http://Maud.Radiographema.Eu/*.
(44) Gu, S.; Fu, B.; Fujita, T.; Ahn, J. W. Thermodynamic Simulations for Determining the Recycling Path of a Spent Lead-Acid Battery Electrolyte Sample with Ca(OH)2. *Appl. Sci.* **2019**, *9* (11), 2262. https://doi.org/10.3390/app9112262.
(45) Beuvier, T.; Bardeau, J.-F.; Calvignac, B.; Corbel, G.; Hindré, F.; Grenèche, J.-M.; Boury, F.; Gibaud, A. Phase Transformations in $CaCO_3$ /Iron Oxide Composite Induced by Thermal Treatment and Laser Irradiation: Phase Transformations in $CaCO_3$ /Iron Oxide Composite. *J. Raman Spectrosc.* **2013**, *44* (3), 489–495. https://doi.org/10.1002/jrs.4200.
(46) Girard, E.; Tassaing, T.; Marty, J.-D.; Destarac, M. Structure–Property Relationships in CO_2 -Philic (Co)Polymers: Phase Behavior, Self-Assembly, and Stabilization of Water/CO_2 Emulsions. *Chem. Rev.* **2016**, *116* (7), 4125–4169. https://doi.org/10.1021/acs.chemrev.5b00420.
(47) Bandyopadhyaya, R.; Kumar, R.; Gandhi, K. S. Modelling of $CaCO_3$ Nanoparticle Formation During Overbasing of Lubricating Oil Additives. *Langmuir* **2001**, *17* (4), 1015–1029. https://doi.org/10.1021/la000023r.
(48) Page, M. G.; Cölfen, H. Improved Control of $CaCO_3$ Precipitation by Direct Carbon Dioxide Diffusion: Application in Mesocrystal Assembly. *Cryst. Growth Des.* **2006**, *6* (8), 1915–1920. https://doi.org/10.1021/cg060152r.
(49) Wang, S.-S.; Picker, A.; Cölfen, H.; Xu, A.-W. Heterostructured Calcium Carbonate Microspheres with Calcite Equatorial Loops and Vaterite Spherical Cores. *Angew. Chem. Int. Ed.* **2013**, *52* (24), 6317–6321. https://doi.org/10.1002/anie.201301184.
(50) Hardikar, V. V.; Matijević, E. Influence of Ionic and Nonionic Dextrans on the Formation of Calcium Hydroxide and Calcium Carbonate Particles. *Colloids Surf. Physicochem. Eng. Asp.* **2001**, *186* (1–2), 23–31. https://doi.org/10.1016/S0927-7757(01)00479-4.